Max-Planck-Institut für Meteorologie

REPORT No. 251

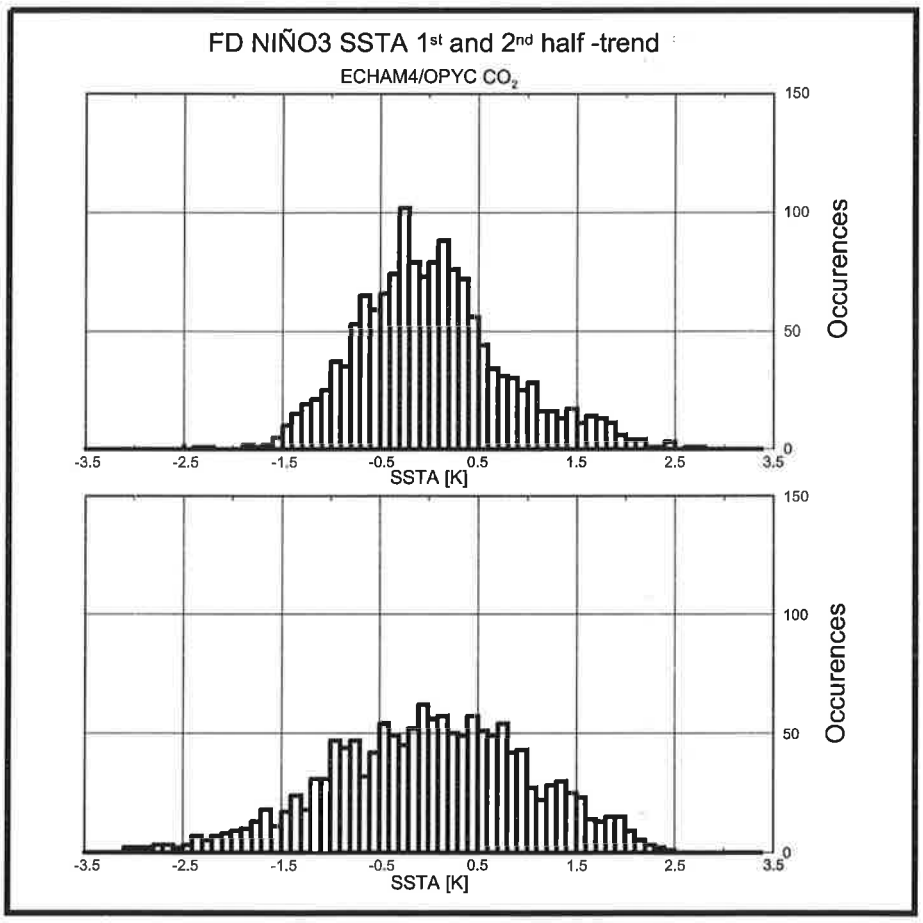

ENSO RESPONSE TO GREENHOUSE WARMING

by

Axel Timmermann • Josef Oberhuber • Andreas Bacher
Monika Esch • Mojib Latif • Erich Roeckner

HAMBURG, February 1998

AUTHORS:

Axel Timmermann
Andreas Bacher
Monika Esch
Mojib Latif
Erich Roeckner

Max-Planck-Institut
für Meteorologie

Josef Oberhuber

DKRZ
Deutsches Klimarechenzentrum
Bundesstr. 55
D-20146 Hamburg
Germany

MAX-PLANCK-INSTITUT
FÜR METEOROLOGIE
BUNDESSTRASSE 55
D - 20146 HAMBURG
GERMANY

Tel.: +49-(0)40-4 11 73-0
Telefax: +49-(0)40-4 11 73-298
E-Mail: <name> @ dkrz.de

ISSN 0937-1060

ENSO Response to Greenhouse Warming

A. Timmermann, J. Oberhuber[1)], A. Bacher, M. Esch, M. Latif, E. Roeckner

Max-Planck-Institut für Meteorologie, Bundesstr. 55, D-20146 Hamburg, Germany

[1)]Deutsches Klimarechenzentrum, Bundesstr. 55, D-20146 Hamburg, Germany

The response of the tropical Pacific climate system and its interannual variability to enhanced greenhouse warming was investigated by means of integrations with a global climate model. The climate model is the first one applied to transient greenhouse warming simulations which simulates the El Niño/Southern Oscillation (ENSO) phenomenon, the leading mode of interannual variability, realistically. The long-term changes in the mean state of the tropical Pacific climate system are similar to those observed during present-day El Niños. Furthermore, the changes in the mean state lead to changes in the statistics of the interannual variability. An ENSO mode exists under enhanced greenhouse conditions also, but it becomes more energetic relative to present, so that variations from year to year become more extreme. In particular, the cold phases of the ENSO cycle amplify considerably, while the statistics of the warm phases do not change significantly. It is shown that changes in the ocean dynamics associated with a sharper thermocline lead to the enhanced interannual variability.Our results have strong implications not only for the global climate system but also for the ecology of the tropical Pacific and the societies and economies of many countries.

submitted to Nature
6/3/98

ISSN 0937-1060

The El Niño/Southern Oscillation (ENSO) phenomenon is the strongest natural interannual climate fluctuation [1]. Although ENSO originates in the tropical Pacific and has large impacts on its ecology, it encompasses the entire global climate system and affects the societies and economies of many countries [2]. ENSO can be understood as an irregular low-frequency oscillation between a warm (El Niño) and a cold state (La Niña). The strong El Niños of 1982/1983 and 1997/1998 and the more frequent occurrences of El Niños during the last few decades raise the question whether greenhouse warming will affect ENSO (e. g. [3]). So far, global climate models that were applied to transient greenhouse warming simulations could not address this question adequately, since they could not simulate ENSO realistically due to their coarse equatorial resolution[4-6].

Our study is the first in which a global climate model which simulates ENSO realistically has been applied to a transient greenhouse warming simulation . The model simulates an irregular ENSO cycle very similar to the observed one (Fig. 1), and the dynamics of the simulated ENSO cycle are consistent with those derived from observations [7-8]. Furthermore, our model succesfully predicted the onset of the El Niño 1997/1998 several months in advance (Fig. 2) [9]. To our knowledge, this is the first global climate model which has been applied to both ENSO predictions and transient greenhouse warming simulations. The climate model is a global coupled ocean-atmosphere-sea ice model that is described in detail in [7-8]. Two experiments were performed with the model. The first experiment is a 240-year long control integration with fixed present-day concentrations of greenhouse gases. The second experiment is a transient greenhouse warming simulation in which the model was forced by increasing levels of greenhouse gases according to IPPC scenario IS92a [10]. The transient integration starts in 1860 and ends in 2100.

The changes in the mean state at the surface of the tropical Pacific as derived from the transient greenhouse warming simulation are reminiscent of the anomalous climate state observed during present-day El Niño conditions (Fig. 3a). In order to describe the changes in the mean state, we computed linear trends of selected variables from the complete transient integration. The SST trend pattern is characterized by a warming of the equatorial east Pacific, which is accompanied by westerly near-surface wind anomalies in the equatorial region to the west of the maximum warming (Fig. 3a). Strong equatorward flow is found off the equator. The associated trend in rainfall is rather similar to the rainfall pattern simulated during present-day El Niños (not shown). The changes in eastern equatorial SST until the end of the next century are found to be as strong as during moderate present-day El Niño events. Since the changes in SST, wind and rainfall are very similar to those oberved during present-day El Niños, it is likely that similar processes to those involved in generating the interannual variability are responsible for the changes in the mean state, as proposed by [11-12].

There has been some discussion about the relative roles of different feedbacks involved in the response of the tropical Pacific to greenhouse warming. On the one hand, it has been argued that the regional differences in the cloud-albedo feedback will lead to a differential surface warming that is centered in the equatorial east Pacific [13]. The argument is that the equatorial west Pacific is so warm that an even modest additional warming would lead to a cloud shielding effect (through high cirrus clouds), reducing the incoming solar radiation at the surface and inhibiting further warming [14]. This 'thermostat' would be less efficient in the eastern equatorial Pacific, so that the eastern Pacific would warm more relative to the western Pacific. This would lead to a slackening of the winds along the equator and to overall conditions very similar to those observed during El Niños. Apparently, this scenario applies in our greenhouse warming simula-

tion.

On the other hand, it has been argued that the strong equatorial upwelling in the eastern equatorial Pacific will weaken the warming in this region, so that the western equatorial Pacific will become warm relative to the eastern equatorial Pacific [15]. This would lead to stronger winds along the equator, to enhanced equatorial upwelling in the eastern Pacific and a net cooling of the eastern and central equatorial Pacific. This 'dynamical thermostat' will lead to overall conditions which will resemble those observed during La Niña episodes, eventually retarding global warming. Since our climate model includes both types of feedbacks, we conclude that the cloud-albedo feedback is the more important one. As discussed by [15], global climate models applied so far to greenhouse warming simulations could not address this problem adequately, since they did not resolve the equatorial upwelling. Our climate model employs a north-south resolution of 0.5° in its ocean component, which is sufficient to resolve the equatorial upwelling. Furthermore, as shown above, our model simulates ENSO realistically and predicted the onset of the 1997/1998 El Niño correctly.

We turn now to the impact of greenhouse warming on the interannual variability in the tropical Pacific. As can be seen from the time evolution of the eastern equatorial SST in the transient greenhouse warming simulation, there is considerable interannual variability superimposed on the warming trend. Our model simulates an irregular ENSO cycle under enhanced greenhouse conditions, with a main period close to that derived from the control integration. The ENSO cycle, however, evolves under different mean conditions (e. g. a warmer climate and a reduced SST gradient along the equator) relative to present, and we therefore may expect that the statistics of the ENSO cycle to change under enhanced greenhouse conditions. A visual inspection of the SST time series (Fig. 4) reveals that the level of the interannual variability increases strongly towards the end of the greenhouse warming simulation. This is also seen in the time series of the interannual SST standard deviations, which shows a statistically significant increase towards the end of the transient greenhouse warming integration (Fig. 5a). Interestingly, the observations also show an intensification of the interannual variability during the last several decades (Fig. 5a). However, as the internally generated fluctuations in the strength of the interannual variability are relatively large, it will be difficult to attribute this to anthropogenic greenhouse warming in the presence of the strong background noise. We note one further interesting feature. The changes in the strength of the interannual variability do not evolve smoothly with time. Instead, the climate model simulates sudden transitions from one regime to the other. Such 'regime shifts' were simulated in the years 1980 and 2060. The observations show an indication for such a 'regime shift' in 1970 (Fig. 5a).

In order to investigate the changes in the ENSO statistics further, we computed the frequency distributions of monthly SST anomalies [16]. The distribution obtained from the first half of the transient integration is narrower than that obtained from the second half. Thus, the year-to-year variability becomes more extreme under enhanced greenhouse conditions. Furthermore, while the distributions of the SST anomalies in the control integration (not shown) and during the first half of the transient integration are almost symmetric (Fig. 4c), the distribution for the second half of the transient integration exhibits a remarkable skewness: Strong cold extremes become more frequent, while the statistics of the strong warm extremes do not change (Fig. 4d).

What causes the changes in the statistics of the interannual variability? On the one hand, the changes in the mean state near the surface (Fig. 3a) could favour a reduction in the ENSO-type variability, since the zonal asymmetries across the equatorial Pacific are reduced [17]. On the other hand, air-sea interactions may become more energetic in a warmer climate, which may

enhance the level of the interannual variability. Finally, the changes in the vertical density structure of the ocean may alter the level of the interannual variability. The equatorial thermocline becomes stronger in response to greenhouse warming (Fig. 3b). Temperatures near the surface warm, while they cool at deeper ocean levels. In order to gain further insight into the dynamics of the changes in the ENSO statistics, we computed atmospheric and oceanic sensitivities as functions of time. The most important atmospheric forcing for equatorial oceans is the zonal wind stress component. We computed first the sensitivity of central equatorial zonal wind stress anomalies to the SST anomalies in the eastern equatorial Pacific averaged over the Niño-3 region (150°W-90°W, 5°N-5°S). No significant change was found (Fig. 5b). We computed next the sensitivity of Niño-3 SST anomalies to changes in the central equatorial zonal wind stress. This exhibited a significant increase towards the end of the transient greenhouse warming simulation, indicating that the changes in the ocean dynamics arising from the strengthening thermocline are responsible for the enhanced interannual variability. This result is consistent with findings obtained from simpler coupled models [18-20].

The simple models also predict a skewness in the frequency distribution of the thermocline depth anomalies in the eastern equatorial Pacific (a quantity closely related to eastern equatorial SST anomalies) for a sharpening thermocline, in the sense that strong cold events become more frequent [20]. This is consistent with our greenhouse warming simulation (Fig. 4). Thus, we conclude that the most important change in the mean state of the tropical Pacific ocean-atmosphere system affecting the ENSO statistics appears to be the strengthening of the equatorial thermocline.

In summary, the tropical Pacific climate system is predicted to undergo strong changes, if emissions of greenhouse gases continue to increase. The climatic effects will be three-fold. First, the mean climate in the tropical Pacific region will change towards a state corresponding to present-day El Niño conditions. It is therefore likely that impacts typical for El Niño will become also more frequent. Secondly, a stronger interannual variability will be superimposed on the changes in the mean state, so that year-to-year variations may become more extreme under enhanced greenhouse conditions. Thirdly, the interannual variability will be more strongly skewed, strong cold events (relative to the warmer mean state) becoming more frequent. These climatic changes can be expected to have strong impacts on the ecology of the tropical Pacific and the societies and economies of many countries.

References

[1] Philander, S. G. H. 1990: El Niño, La Niña, and the Southern Oscillation. Academic Press, 293 pp.

[2] Glantz, M. H., R. W. Katz and N. Nicholls, 1991: Teleconnections linking worldwide climate anomalies. Cambridge University Press, 535 pp.

[3] Trenberth K. and T. Hoar, 1996: The 1990-1995 El Niño-Southern Oscillation event: Longest on record. Geophys. Res. Lett., 23, 57-60.

[4] Knutson, T. R., S. Manabe, and D. Gu, 1997: Simulated ENSO in a Global Coupled Ocean-Atmosphere Model: Multidecadal Amplitude Modulation and CO_2 Sensitivity. J. Climate, 10. 138-161.

[5] Tett, S. , 1995: Simulation of El Niño-Southern Oscillation-like variability in a global AOGCM and its response to CO_2 increase. J. Climate, 8, 1473-1502.

[6] Meehl, G. A., G. W. Brantstator, and W. M. Washington, 1993: Tropical Pacific interannual variability and CO_2 climate change. J. Climate, 6, 42-63.

[7] Roeckner, E., J. M. Oberhuber, A. Bacher, M. Christoph, and I. Kirchner, 1996: ENSO variability and atmospheric response in a global atmosphere-ocean GCM. Climate Dynamics, 12, 737-754.

[8] Bacher, A. , J. M. Oberhuber, and E. Roeckner, 1997: ENSO dynamics and seasonal cycle in the tropical Pacific as simulated by the ECHAM4/OPYC3 coupled general circulation model. Climate Dynamics, in press.

[9] The forecast experiments and the initialization strategy are described in Oberhuber et al. 1998 (to be submitted to Geophysical Research Letters). The forecast experiments were conducted as follows: The observed SST anomalies were used to force the global climate model up to the prediction start time. Thereafter the climate model evolves freely in the forecast mode. The forecasts were made in ensemble mode, and all members of the ensemble reproduced well the observations.

[10] IPCC, 1992: Climate Change 1992. The Supplementary Report to the IPCC Scientific Assessment. Edited by J. T. Houghton, B. A. Callander and S. K. V. Varney. Cambridge University Press, 200 pp.

[11] Dijkstra, H. A. and J. D. Neelin, 1995: Ocean-atmosphere interaction and tropical climatology. Part II: Why the Pacific cold tongue is in the east. J. Climate, 8, 1343-1359.

[12] Bjerknes, J., 1969: Atmospheric teleconnections from the equatorial Pacific. Mon. Wea. Rev., 97, 163-172.

[13] Meehl, G. A. and W. M. Washington, 1996: El Niño-like climate change in a model with increased atmospheric CO_2 concentrations. Nature, 382, 56-60.

[14] Ramanathan, V. and W. Collins, 1991: Thermodynamic regulation of ocean warming by cirrus clouds deduced from observations of the 1987 El Niño. Nature, 351, 27-32.

[15] Cane, M. A., A. C. Clement, A. Kaplan, Y. Kushnir, D. Pozdnyakov, R. Seager, S. E. Zebiak, and R. Murtugudde, 1997: Twentieth-century sea surface temperature trends. Science, 275, 957-960.

[16] Anomalies were computed by subtracting the linear trends and means from the time series of eastern equatorial Pacific SSTs and by removing the mean annual cycle of the control integration.

[17] Battisti, D. S. and A. C. Hirst, 1989: Interannual variability in the tropical atmosphere/ ocean system: Influence of the basic state, ocean geometry and non-linearity. J. Atmos. Sci., 46, 1687-1712.

[18] Münnich, M., M. A. Cane and S. E. Zebiak 1991: A Study of Self-excited Oscillations of the Tropical Ocean-Atmosphere System, Part II: Nonlinear Cases, J. Atm. Sci., 48, 1238-1248.

[19] Tziperman, E., L. Stone, M. A. Cane and H. Jarosh 1994: El Niño Chaos: Overlapping of Resonances Between the Seasonal Cycle and the Pacific Ocean-Atmosphere Oscillator, Science 264,72-74.

[20] L. Stone, P.I. Saparin, A. Huppert and C. Price 1998: El Niño Chaos: The potential role of noise and stochastic resonance on the ENSO cycle. Geophy. Res. Letters, 25, 175-178.

Acknowledgements. We would like to thank Dr. T. P. Barnett for many stimulating discussions and Dr. M. Münnich for helping with the data processing. This work was sponsored by the German government under its programme 'Klimavariabilität und Signalanalyse'. The climate model integrations were performed at the Deutsches Klimarechenzentrum.

Correnspondence and requests for materials should be addressed to M. L.
(e-mail: latif@dkrz.de)

Figure Captions

Fig. 1: Comparison of the interannual variability of SST as observed and simulated by the global climate model. a) Standard deviations of observed monthly SST anomalies for the period 1949-1994. b) Standard deviations of simulated monthly SST anomalies as derived from the 240-year long control integration with the global climate model. Linear trends were removed prior to both analyses. The units are ^{o}C.

Fig. 2: Observed (a) and by the global climate model predicted (b) tropical Pacific SST anomalies for July 1997 (^{o}C). The climate model was initialized by assimilating observed SST anomalies until December 1996. Thus, the model prediction represents a forecast 7 months in advance.

Fig. 3: a) Linear trends in SST (^{o}C/100 years) and near-surface winds [(m/s)/100 years] as derived from the full (240-years long) transient greenhouse warming simulation. Note the relatively strong warming trend in the eastern equatorial Pacific, which is accompanied by westerly wind anomalies. These trends resemble the anomalous conditions observed during present-day El Niños. b) Linear trends in the temperatures of the upper 210 meters of the ocean at the equator (^{o}C/100 years) as derived from the full (240-years long) transient greenhouse warming simulation. Note the warming trend near the surface and the cooling trend at deeper levels leading to a stronger thermocline.

Fig. 4: Time series of eastern equatorial SST anomalies (relative to the control run) averaged over the Niño-3 region (150^{o}W-90^{o}W, 5^{o}N-5^{o}S) (^{o}C) during the first half (panel a) and second half (panel b) of the transient greenhouse warming simulation. Frequency distribution of Niño-3 SST anomalies during the first half (panel c) and second half (panel d) of the transient greenhouse warming simulation. The frequency distributions were calculated after subtracting the linear trends. Note the change in the frequency distributions from the first to the second half of the transient integration. While the distribution is almost symmetric during the first half (and during the control integration, not shown), the distribution is biased towards the 'cold side' during the second half of the transient integration: strong cold events become more frequent.

Fig. 5: a) Standard deviations of Niño-3 SST anomalies (^{o}C) as function of time during the transient greenhouse warming simulation (black curve). Also shown is the time evolution of the standard deviation of the observed Niño-3 SST anomalies (red curve). A low-pass filter in the form of a sliding window of 10 years width was used to compute the standard deviations. Both the simulated and observed SST anomalies exhibit trends towards stronger interannual variability. The standard deviations in the transient warming simulation leave the 2σ confidence level (dashed black lines, derived from the control integration with present-day concentrations of greenhouse gases) towards the end of the transient integration.

b) Sensitivity of central equatorial zonal wind stress anomalies (averaged over the region 100^{o}W-160^{o}W, 1.4^{o}N-1.4^{o}S) to changes in Niño-3 SST anomalies as function of time during the transient greenhouse warming simulation (black curve). The atmospheric sensitivity is defined as the covariance of the zonal wind stress and Niño-3 SST anomalies divided by the variance of the Niño-3 SST anomalies (Pa/^{o}C). Also shown is the sensitivity of eastern equatorial SST anomalies averaged over the Niño-3 region to the central equatorial zonal wind stress anomalies averaged over the region indicated above (red curve). The oceanic sensitivity is defined as the covariance of the zonal wind stress and Niño-3 SST anomalies divided by the variance of the zonal wind stress anomalies (^{o}C/Pa). A sliding window of 10 years width was used to compute the sensitivities. The 2σ limits derived from the control run are shown by the dashed black and red lines, respectively.

Fig. 1 a)

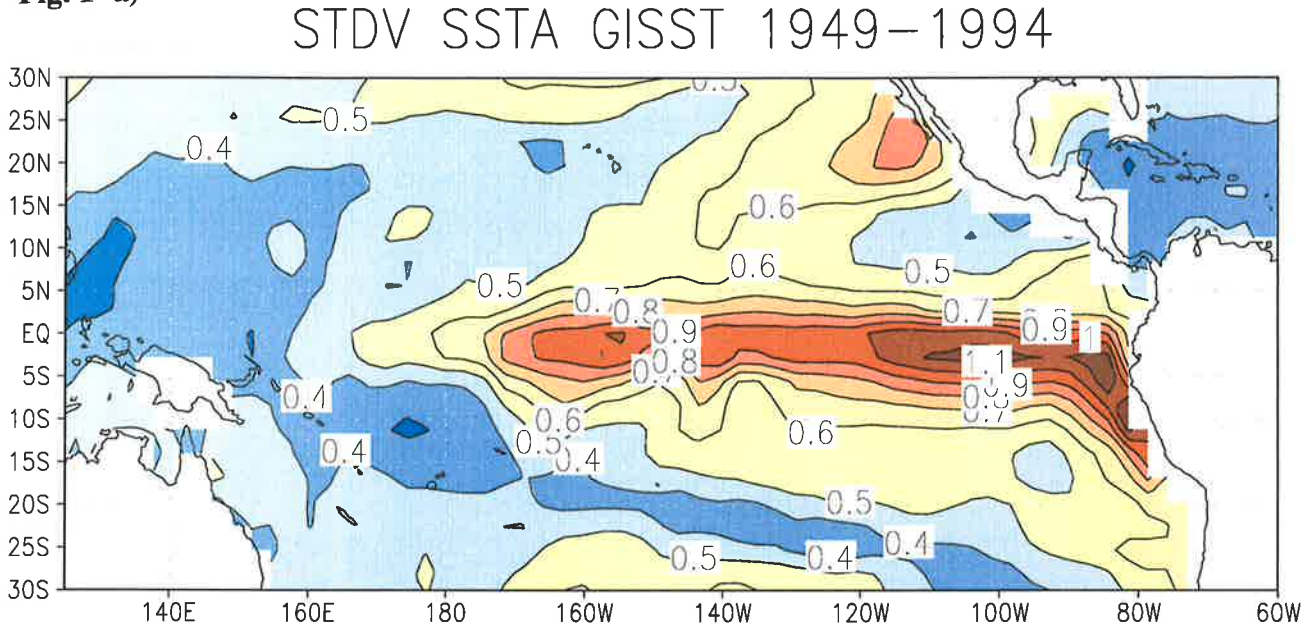
STDV SSTA GISST 1949–1994
30N
25N
20N
15N
10N
5N
EQ
5S
10S
15S
20S
25S
30S
140E
160E
180
160W
140W
120W
100W
80W
60W

Fig. 1 b)

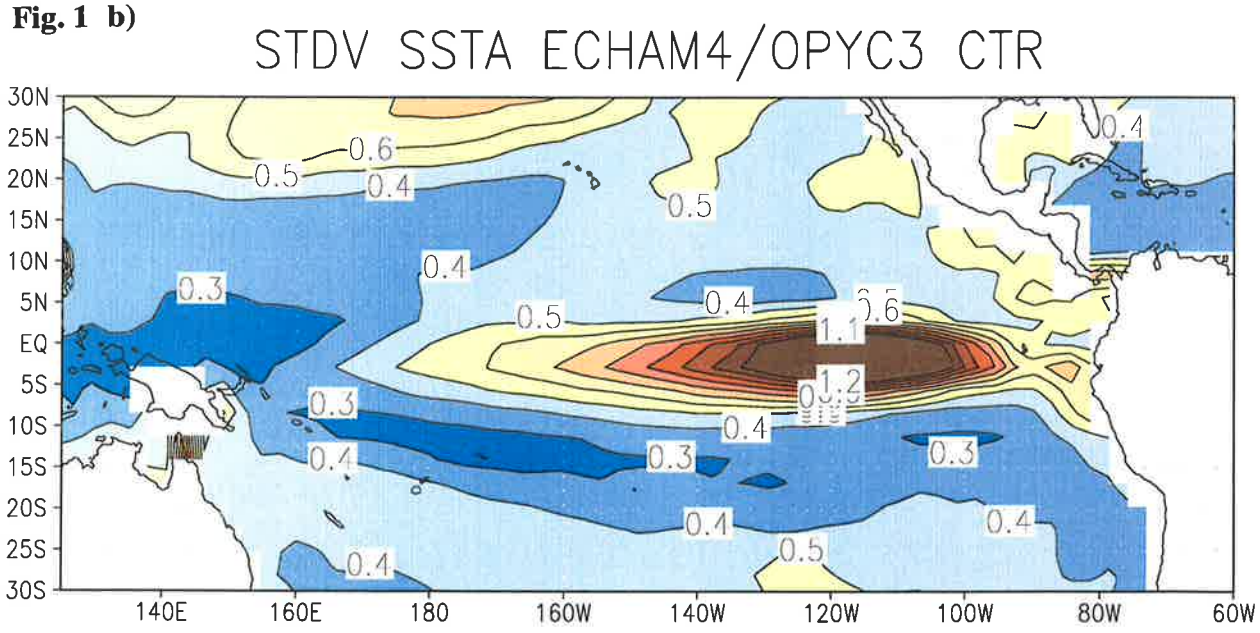
STDV SSTA ECHAM4/OPYC3 CTR
30N
25N
20N
15N
10N
5N
EQ
5S
10S
15S
20S
25S
30S
140E
160E
180
160W
140W
120W
100W
80W
60W

Fig. 2 a)

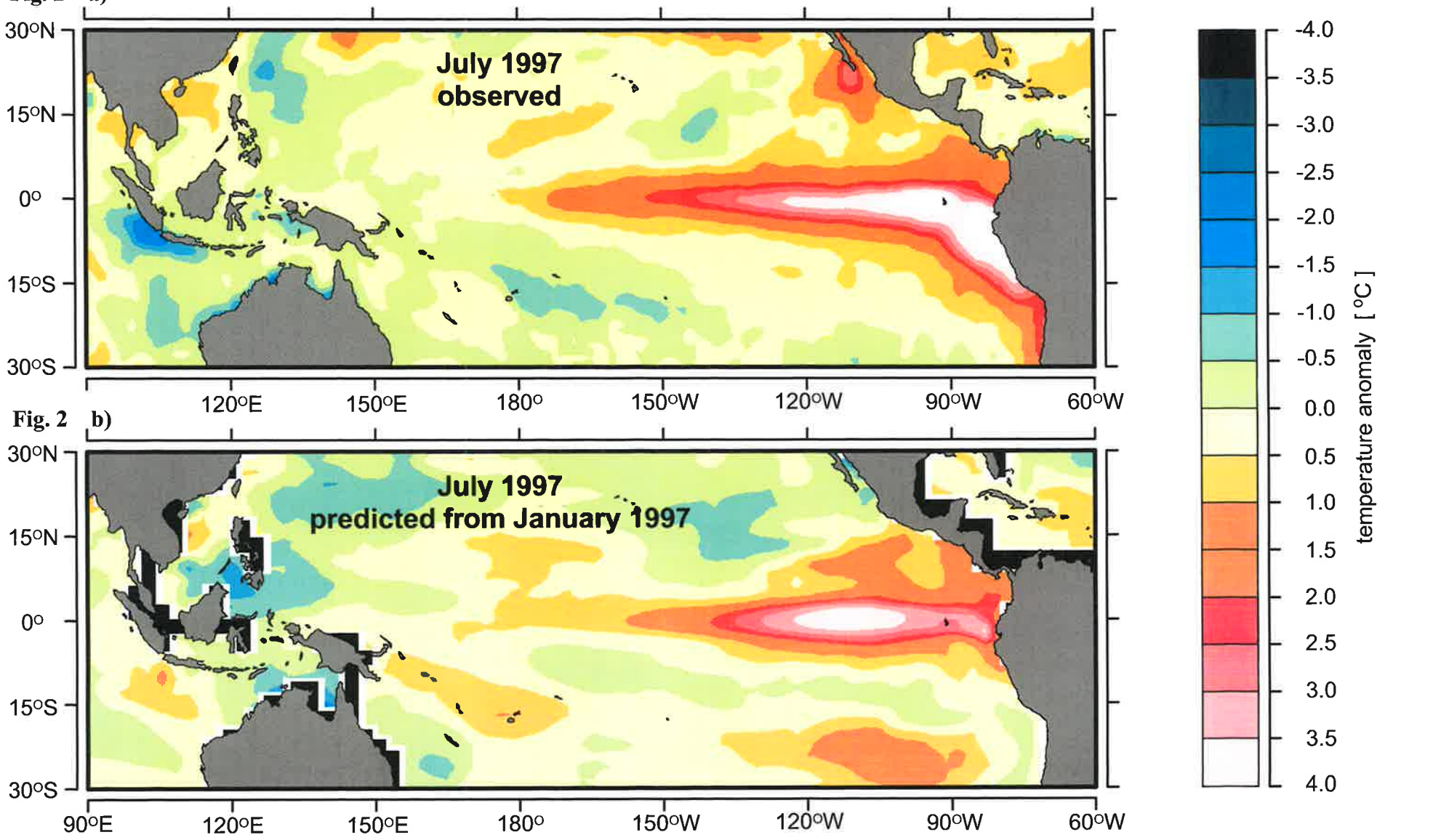

Fig. 2 b)

028MOLa.dsf

Fig. 3 a)

Trend SSTA, 10m winds, T(x,z) eq. ECHAM4/OPYC3 CO2

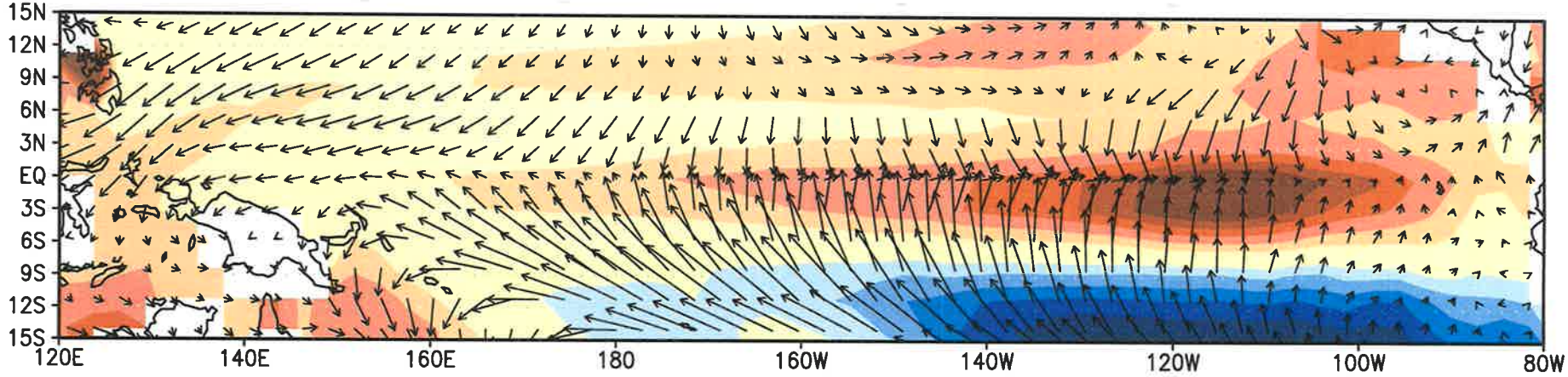

Fig. 3 b)

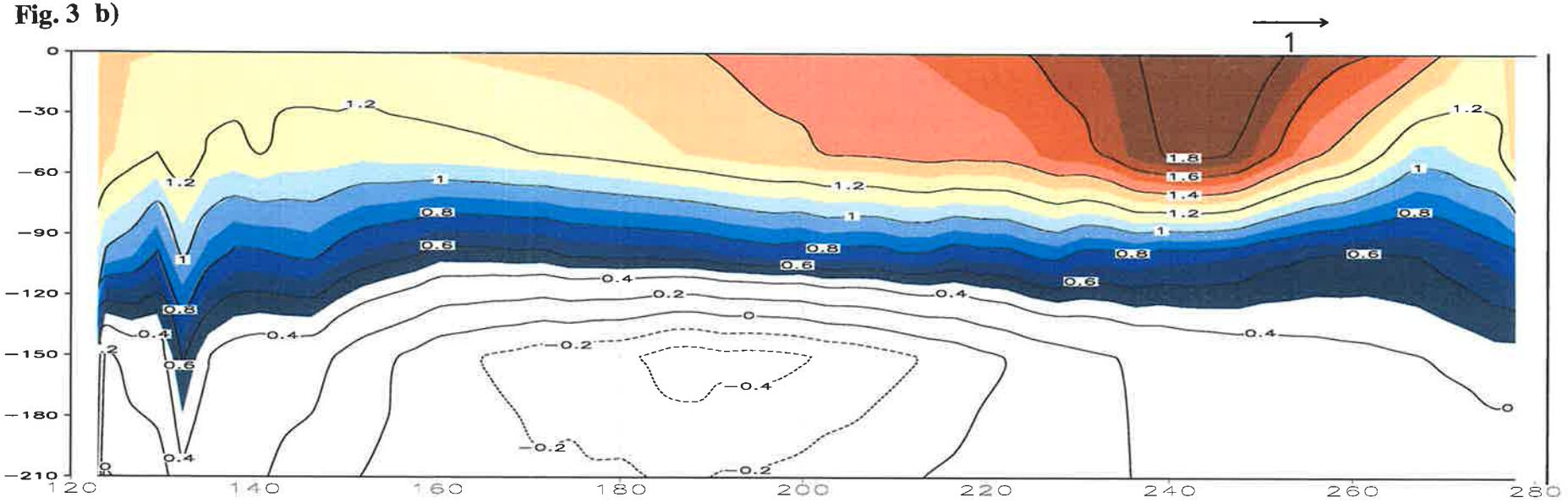

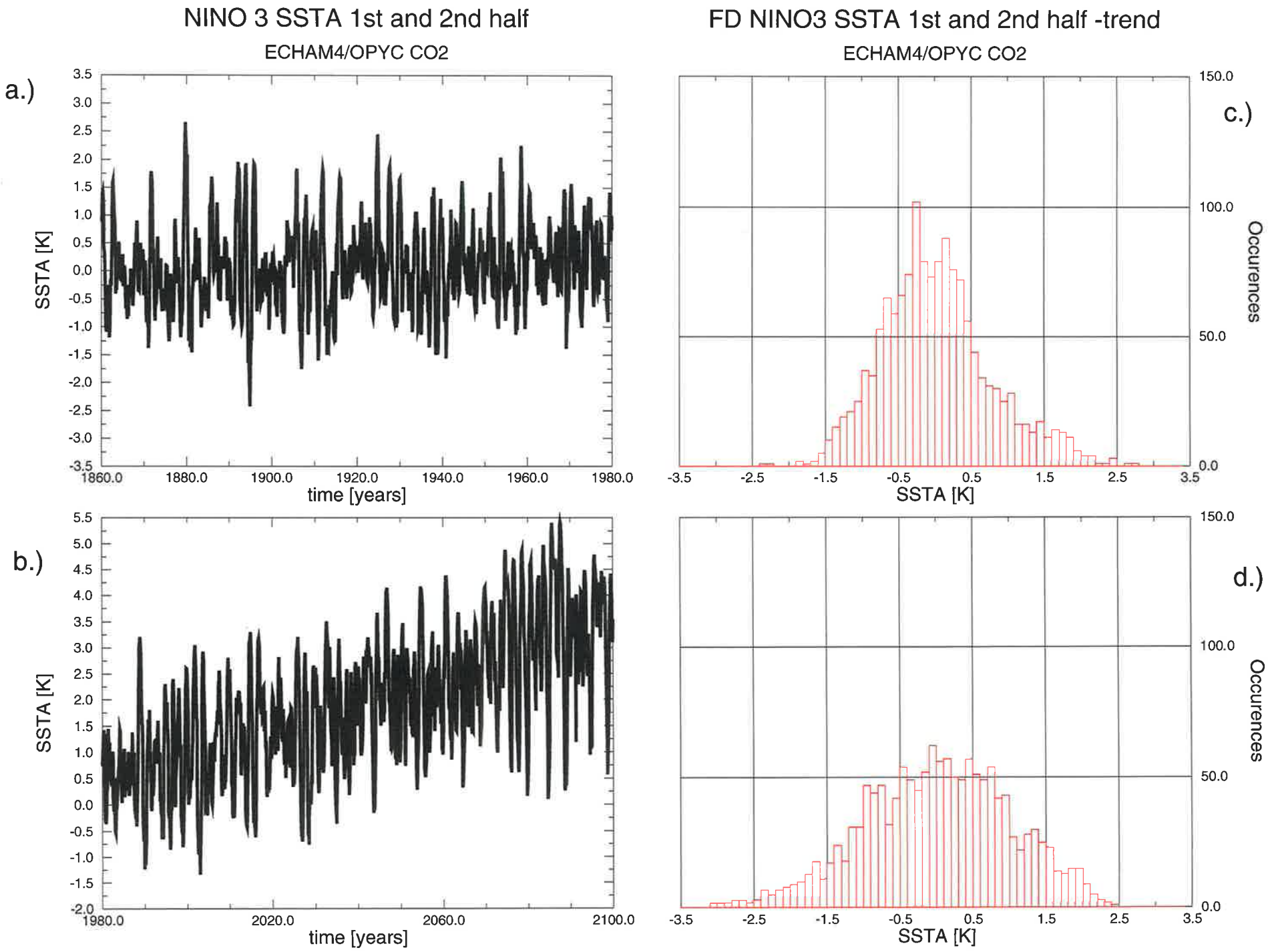
NINO 3 SSTA 1st and 2nd half
ECHAM4/OPYC CO2
a.)
SSTA [K]
time [years]
b.)
SSTA [K]
time [years]
FD NINO3 SSTA 1st and 2nd half -trend
ECHAM4/OPYC CO2
c.)
Occurences
SSTA [K]
d.)
Occurences
SSTA [K]

Fig. 5 a)

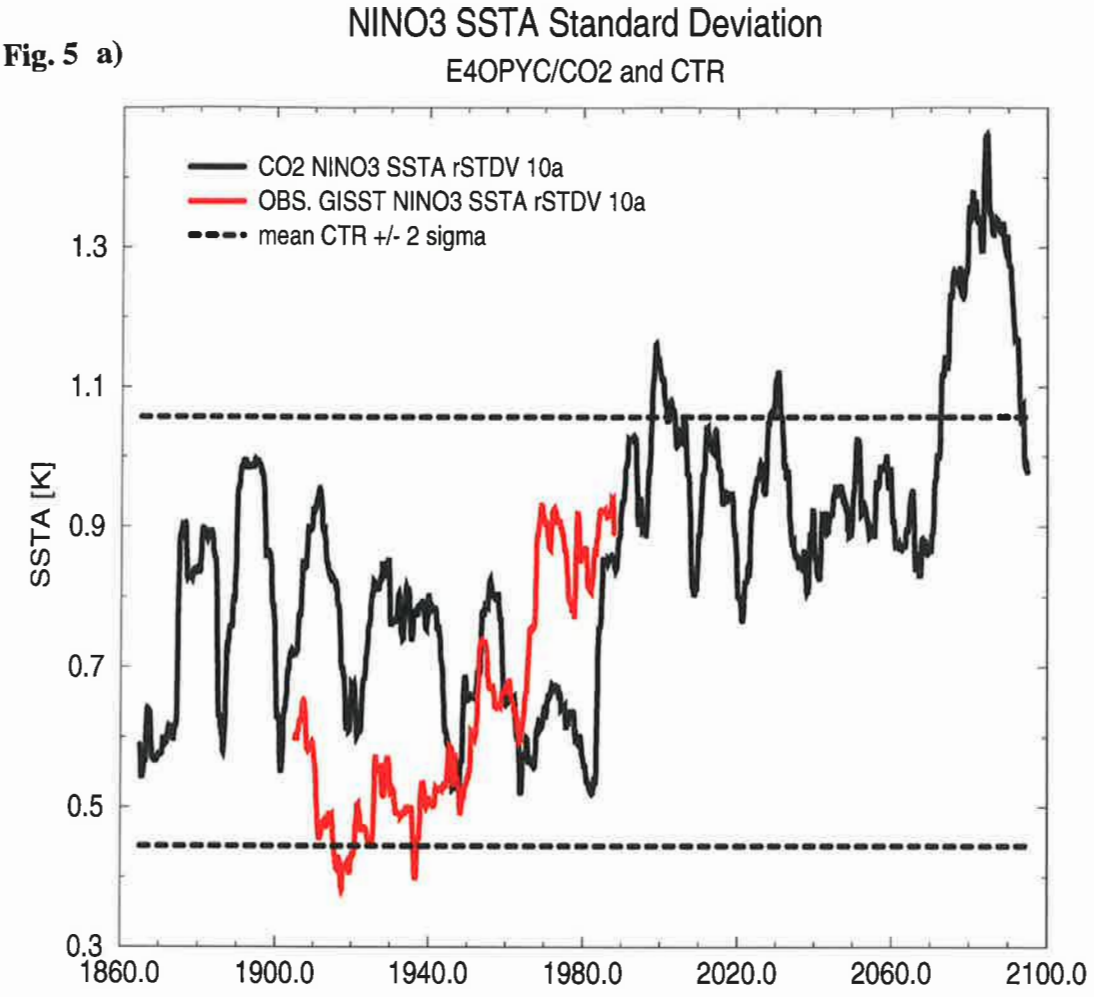
NINO3 SSTA Standard Deviation
E4OPYC/CO2 and CTR
CO2 NINO3 SSTA rSTDV 10a
OBS. GISST NINO3 SSTA rSTDV 10a
mean CTR +/- 2 sigma
SSTA [K]
1.3
1.1
0.9
0.7
0.5
0.3
1860.0
1900.0
1940.0
1980.0
2020.0
2060.0
2100.0

Fig. 5 b)

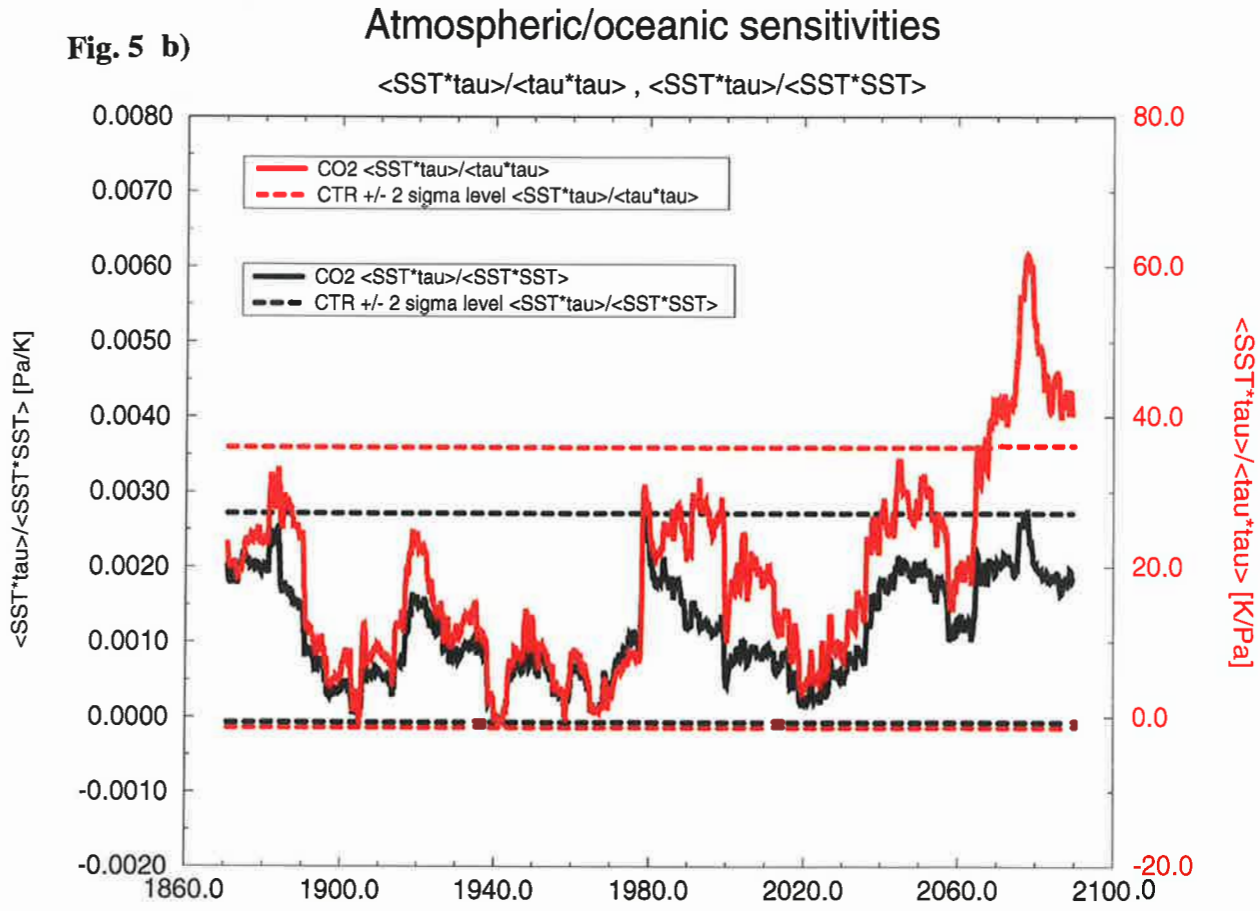
Atmospheric/oceanic sensitivities
<SST*tau>/<tau*tau> , <SST*tau>/<SST*SST>
CO2 <SST*tau>/<tau*tau>
CTR +/- 2 sigma level <SST*tau>/<tau*tau>
CO2 <SST*tau>/<SST*SST>
CTR +/- 2 sigma level <SST*tau>/<SST*SST>
<SST*tau>/<SST*SST> [Pa/K]
<SST*tau>/<tau*tau> [K/Pa]
0.0080
0.0070
0.0060
0.0050
0.0040
0.0030
0.0020
0.0010
0.0000
-0.0010
-0.0020
80.0
60.0
40.0
20.0
0.0
-20.0
1860.0
1900.0
1940.0
1980.0
2020.0
2060.0
2100.0